ACS Catalysis

pubs.acs.org/acscatalysis

Research Article

High Propylene Selectivity in Methanol Conversion over a Small-Pore SAPO Molecular Sieve with Ultra-Small Cage

Miao Yang, Bing Li, Mingbin Gao, Shanfan Lin, Ye Wang, Shutao Xu, Xuebin Zhao, Peng Guo, Yingxu Wei, Mao Ye, Peng Tian,* and Zhongmin Liu*

Cite This: *ACS Catal.* 2020, 10, 3741−3749

Read Online

ACCESS | Metrics & More | Article Recommendations | Supporting Information

ABSTRACT: Conversion of methanol to olefins (MTO) is an important non-oil alternative route for ethylene and propylene production, which has been industrialized based on a fluidized-bed process with a small-pore SAPO-34 (CHA topology) molecular sieve as the active catalyst component. However, it remains a challenge to effectively regulate the selectivity toward single ethylene or propylene due to the limited catalyst selection and insufficient understanding of the selectivity control principle. Herein, we report the synthesis of a small-pore SAPO-14 molecular sieve (AFN topology) with an ultra-small cage structure and a narrow 8-membered ring (8-MR) channel system, over which the propylene selectivity can rise to as high as 77.3%, representing the highest record of one-pass propylene selectivity in the MTO reaction. The influence of reaction conditions on the catalytic performance was investigated, and the olefin formation mechanism was revealed by combining the analyses of $^{12}C/^{13}C$-methanol isotopic switch experiments, confined organics analysis, and reaction-diffusion simulations. This work provides a possibility to subtly control the MTO product distribution by the design and synthesis of the molecular sieve catalyst.

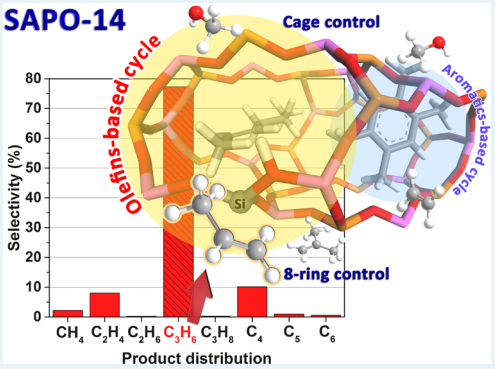

KEYWORDS: *SAPO molecular sieve, ultra-small cage, methanol to propylene, hydrothermal synthesis, shape selective catalysis*

1. INTRODUCTION

Propylene, as one of the most important building blocks of petrochemicals, has huge global demands far from being met by conventional propylene production through steaming cracking and catalytic cracking of naphtha. Methanol to olefins (MTO), as a competitive nonpetroleum route to produce light olefins, draws considerable attention since the low-cost coal or natural gas can be easily converted to methanol.[1] Small-pore silicoaluminophosphate (SAPO) molecular sieves like SAPO-34 and SAPO-18 have high light olefins selectivity, which are considered as excellent MTO catalysts. However, the product distribution of ethylene and propylene over them is close. To maximize the propylene production, the methanol to propylene (MTP) process was especially developed, wherein the olefin-containing stream other than propylene undergoes recirculations.[2−5] The catalyst with a high one-pass propylene selectivity and high propylene to ethylene (P/E) ratio is thus highly desirable.

The zeolite catalyst is one of the most important decisive factors to control the product selectivity of the MTO reaction, whose framework structure and composition (acidity), together with reaction conditions, determine the formation of reaction intermediates, reaction routes, and product selectivity.[6−10] Considerable efforts have been devoted to screen and optimize the zeolite catalyst with the aim to manipulate the product distribution. The principle behind the selectivity control is mainly based on the dual-cycle mechanism first proposed on the ZSM-5 catalyst,[11,12] which considers that ethylene mainly comes from the aromatics cycle, while propylene and higher alkenes are generated from the olefins cycle, that is alkene methylations and cracking reactions. Further research reveals that the ratio of the double cycle can be modified through controlling the internal reaction space (cavity or channel intersection) of the zeolite catalyst, which determines the size of the active intermediates and thus the product selectivity.[13,14] With the increase of internal space, the size of the formed methylbenzenes increases and the preferential product changes from ethylene to propylene and butylene.[8] Besides the zeolite structure, acidity is also an important factor for selectivity optimization. Weaker acid strength and lower acid density favor the olefins cycle and the formation of propylene and higher alkenes.[15]

Received: October 31, 2019
Revised: February 20, 2020
Published: February 26, 2020

https://dx.doi.org/10.1021/acscatal.9b04703
ACS Catal. 2020, 10, 3741−3749

To enhance the propylene selectivity, 10-MR and 12-MR zeolites with a high SiO_2/Al_2O_3 ratio (low acid concentration) have been rationally synthesized to suppress the aromatics cycle and improve the olefins cycle. Over 50% propylene selectivity and a P/E ratio higher than 10 can be realized over the 10-MR high silica ZSM-5 nanosheet (SiO_2/Al_2O_3 = ~400),[16] EU-1 zeolite (SiO_2/Al_2O_3 = ~400),[17] as well as 12-MR CON[18] and β (SiO_2/Al_2O_3 = ~300)[19,20] zeolite catalysts. However, the yield of C_{4+} hydrocarbon products is always larger than 30% because 10-MR and 12-MR zeolite catalysts are conducive to the formation and diffusion of molecules with the larger size. Therefore, it is very difficult to further increase the propylene selectivity even if high reaction temperature (over 500 °C) is used to promote the cracking of higher alkenes.[19] A small-pore molecular sieve with narrow 8-MR pore openings has apparent superiority in light olefin production due to the diffusion limitation imposed by the limited reaction space. In particular, SAPO-18 was reported to have a higher propylene selectivity than SAPO-34 because of the fact that its larger pear-shaped AEI cage favors the formation of higher substituted methylbenzene and pentamethylcyclopentenyl intermediates, leading to increased propylene and butylene products.[21,22] However, the aromatics-based cycle always occupies a higher proportion over SAPO-18 even if its acid density is controlled to be extremely low, resulting in a P/E ratio lower than 2.0.[22,23] This implies the difficulty to restrain the aromatics cycle for cavity-type molecular sieves. The product selectivity can only be slightly altered by modifying the size of 8-MR pore openings. Narrower pore sizes tend to deliver enhanced ethylene and propylene selectivity, yet larger 8-MR pores lead to higher selectivity to the C_{4+} product.[9] The results suggest that controlling the selectivity toward a certain single product is full of challenges. The cavity structure, pore size, and acidity are still important parameters for catalyst design and selectivity control.

In this work, we report for the first time the synthesis and characterization of a small-pore SAPO-14 molecular sieve with AFN topology, which exhibits an unprecedentedly high propylene selectivity and P/E ratio. AlPO-14 is well known due to its excellent gas adsorption/separation ability, especially in propylene/propane separation.[24] However, it is difficult to introduce Si atoms into the AFN framework, so the investigation on SAPO-14 is rare.[25] Herein, SAPO-14 was successfully synthesized and demonstrated to be an efficient catalyst for the MTP reaction owing to its low acid concentration and unique structural feature containing an ultra-small cage and a narrower 8-MR channel system. $^{12}C/^{13}C$-methanol isotopic switch experiments, confined organics analysis, and reaction-diffusion simulations were conducted to investigate/reveal the catalytic reaction pathway and the mechanism of its high propylene selectivity.

2. EXPERIMENTAL SECTION

2.1. Synthesis. For the syntheses of AlPO-14 and SAPO-14, pseudoboehmite (65.5 wt %) was first dissolved in distilled water, and then H_3PO_4 (85 wt %), tetraethyl orthosilicate (TEOS), if necessary, and isopropylamine (IPA) were added in sequence with stirring. The molar compositions of reactant gels were 1.0 Al_2O_3/1.0 P_2O_5/(0−0.18) SiO_2/(1.0−1.4) IPA/(40−75) H_2O. The mixtures were transferred to stainless steel autoclaves and heated to 200 °C for 48 h under rotation. The products were filtered, washed, and dried in air. For comparison, SAPO-18s with a similar Si content were also synthesized according to refs 26, 27. The reactants and synthetic procedures were similar to those of SAPO-14, except for the different organic templates used. The reaction conditions for S5 were 1.0 Al_2O_3/1.0 P_2O_5/0.012 SiO_2/1.73 *N*,*N*-diisopropylethylamine/45H_2O at 160 °C for 36 h under rotation; and the reaction conditions for S6 were 1.0 Al_2O_3/0.9 P_2O_5/0.045 SiO_2/3.5 triethylamine/40 H_2O at 180 °C for 17 h under rotation. After crystallization, the products were filtered, washed, and dried in air.

2.2. Characterization. The powder X-ray diffraction (XRD) patterns were recorded on a PANalytical X'Pert PRO X-ray diffractometer with Cu Kα radiation (λ = 1.54059 Å), operating at 40 kV and 40 mA. The chemical composition of the samples was determined using a Philips Magix-601 X-ray fluorescence (XRF) spectrometer. The crystal morphology was observed by field emission scanning electron microscopy (FESEM, Hitachi SU8020). The transmission electron microscopy (TEM) images and selected area electron diffraction (SAED) patterns were acquired on the JEOL JEM2100 TEM. The textural properties of the calcined samples were determined by N_2 adsorption at 77 K and Ar adsorption at 88 K, respectively, on a Micromeritics ASAP 2020 system. The total surface area was calculated based on the Brunauer−Emmett−Teller (BET) equation. The micropore volume, micropore surface area, and the external surface area were evaluated using the *t*-plot method. The temperature-programmed desorption of ammonia (NH_3-TPD) was carried out with AutochemII2920 equipment (Micromeritics). Then, 0.2 g of the sample particles (40−60 mesh) were loaded into a U-quartz tube and pretreated at 650 °C for 60 min under He flow. After cooling down to 100 °C, a gas mixture of NH_3 and He flow was introduced to saturate the sample with NH_3 adsorption (60 min). After this, He flow was purged through the sample for 30 min to remove the weakly adsorbed NH_3 molecules. The measurement of the desorbed NH_3 was performed from 100 to 600 °C (10 °C/min) under He flow (20 mL/min). The NH_3-TPD experiments were then conducted for a second time using the same procedure, except for changing the initial NH_3 adsorbed temperature to 150 °C. All of the solid-state NMR experiments were performed on a Bruker Avance III 600 spectrometer equipped with a 14.1 T wide-bore magnet. The resonance frequencies were 150.9 156.4, 242.9, and 119.2 MHz for ^{13}C, ^{27}Al, ^{31}P, and ^{29}Si, respectively. All of the NMR experiments were performed on a 4 mm MAS probe with a spinning rate of 12 kHz for ^{13}C, ^{27}Al, and ^{31}P. ^{13}C CP/MAS NMR spectra were recorded with a contact time of 3 ms and a recycle delay of 2 s. ^{27}Al MAS NMR spectra were recorded using one pulse sequence. Two-hundred scans were accumulated with a $\pi/8$ pulse width of 0.75 μs and a 2 s recycle delay. Chemical shifts were referenced to $(NH_4)Al(SO_4)_2 \cdot 12H_2O$ at −0.4 ppm. ^{31}P MAS NMR spectra were recorded using high-power proton decoupling. Thirty-two scans were accumulated with a $\pi/4$ pulse width of 2.25 μs and a 10 s recycle delay. Chemical shifts were referenced to 85% H_3PO_4 at 0 ppm. ^{29}Si CP/MAS NMR spectra were recorded with a contact time of 3 ms and a recycle delay of 2 s with a spinning rate of 8 kHz. Chemical shifts for ^{29}Si were referenced to kaolinite at −91.5 ppm.

2.3. Catalyst Evaluation. Methanol to olefin (MTO) reaction was performed in a quartz tubular fixed-bed reactor at atmospheric pressure. Then, 0.3 g catalyst (40−60 mesh) was loaded in the quartz reactor and activated at 550 °C in a N_2 flow of 30 mL/min for 1 h before starting each reaction run,

https://dx.doi.org/10.1021/acscatal.9b04703
ACS Catal. 2020, 10, 3741−3749

and then the temperature was adjusted to 375−475 °C as required. The methanol was fed by passing N_2 carrier gas with velocities of 44.6, 42.2, and 38.0 mL/min through a saturator containing methanol at 1, 12, and 25 °C, respectively, which gave weight hourly space velocities (WHSV) of 0.5, 1, and 2 h^{-1}, respectively. The reaction products were analyzed using an online gas chromatograph (Agilent GC 7890N), equipped with a flame ionization detector (FID) and a Plot-Q column. Since the catalytic lifetime was short, intermittent sampling was taken if necessary to learn more reaction details. Methanol was first fed for 1 min and then stopped with only N_2 stream passing through the catalyst during GC analysis. When GC analysis was completed and ready for the next sample, the methanol was fed again for the desired time to measure the activity by GC analysis. This operation was repeated until the deactivation of the SAPO-14 catalyst. The time of stream (TOS) was the accumulated methanol feeding time. The distributions of C_4 products at the selective reaction time were sampled separately and analyzed by Agilent GC 7890A equipped with a flame ionization detector (FID) and an Al_2O_3 column.

2.4. $^{12}C/^{13}C$-Methanol Isotopic Switch Experiments. ^{12}C-methanol was first fed at 400 °C and WSHV of 2.0 h^{-1} for 2 min, and then ^{13}C-methanol was fed for another 1 min under the same conditions. The effluent products from the reactor were kept warm and analyzed by an online gas chromatograph (GC) equipped with a PoraPLOT-Q capillary column, an FID detector, and a mass spectrometric detector (Agilent 7890B/5977A). For detecting the organic compounds confined in the catalyst, the above experiment was repeated again. After 1 min ^{13}C-methanol feeding, the catalyst was discharged and placed in a vessel containing liquid nitrogen immediately. Subsequently, 50 mg of catalyst was dissolved in 1 mL of 40% HF solution. The residual organic species in the catalyst were further extracted using 1 mL CH_2Cl_2 with 200 ppm C_2Cl_6 as an internal standard. The organic species were analyzed by GC-MS (Agilent 7890A/5975C MSD) with an HP-5 MS capillary column (30 m × 0.25 mm × 0.25 mm).

2.5. Confined Organics Analysis. The catalyst was first exposed to methanol at 400 °C and WHSV of 2 h^{-1} for 30 min. After cooling down to room temperature, the catalyst was discharged and treated using the same procedure above by HF solution and CH_2Cl_2. The organic species were analyzed by GC-MS (Agilent 7890A/5975C MSD) with an HP-5 MS capillary column (30 m × 0.25 mm × 0.25 mm).

3. RESULTS AND DISCUSSION

3.1. Synthesis and Characterization of SAPO-14. SAPO-14s were synthesized using isopropylamine (IPA) as a template. The synthetic details and results are listed in Table 1. The Si contents of SAPO-14 products are in the range of 0−2.2%. Attempting to further increase the Si dosage in the initial gel results in the presence of SAPO-43 and SAPO-34 impurities, as shown in Table 1 and Figure S1. When the Si content of the gel is over 0.15, the main product becomes SAPO-34 together with some SAPO-14. Figure 1A,B shows the XRD patterns of the as-synthesized and calcined SAPO-14 samples, which are in good agreement with their simulated ones from AlPO-14. The difference between the two XRD patterns should result from the change in atom coordination environments upon calcination, similar to the previous report.[28] The results evidence that the as-synthesized SAPO-14 has an AFN framework topology that has a three-dimensional (3D) interconnecting 8-ring channel system with a slender $4^6 8^8$ AFN cage (5.3 Å × 10.05 Å), as shown in Figure 1C,D. The AFN cage can accommodate a sphere with a maximum diameter of 5.3 Å.[29] This value is big enough for holding a hexamethylbenzene molecule (Figure 1C) but is smaller than those of most small-pore AlPO and SAPO materials. The cage structures of AEI, AFV, AFX, AVL, CHA, ERI, LEV, LTA, RHO, SAV, and SAS topologies can take a sphere with a diameter larger than 7 Å.

Table 1. Molar Compositions of the Initial Gels and the Synthetic Results

		starting gel compositions	product composition[b]
samples	crystalline phase	$Al_2O_3/P_2O_5/SiO_2/R^a/H_2O$	molar composition
S1	AlPO-14	1.0/1.0/0/1.0/50	$Al_{0.502}P_{0.496}Si_{0.002}O_2$
S2	SAPO-14	1.0/1.0/0.08/1.375/75	$Al_{0.502}P_{0.475}Si_{0.022}O_2$
S3	SAPO-14 and minor impurity	1.0/1.0/0.15/1.375/50	$Al_{0.523}P_{0.438}Si_{0.039}O_2$
S4	SAPO-34 and minor SAPO-14	1.0/1.0/0.18/1.375/75	$Al_{0.484}P_{0.454}Si_{0.062}O_2$
S5	SAPO-18	1.0/1.0/0.012/1.73/45	$Al_{0.500}P_{0.494}Si_{0.006}O_2$
S6	SAPO-18	1.0/0.9/0.045/3.5/40	$Al_{0.494}P_{0.485}Si_{0.020}O_2$

[a]R is isopropylamine for S1-S4, *N*,*N*-diisopropylethylamine for S5, and triethylamine for S6, respectively. [b]Determined by X-ray fluorescence (XRF) spectrometry.

The pore size of SAPO-14 is also smaller than those of the other 8-ring molecular sieves, as shown in Figure 1D. N_2 adsorption measurement gives a typical type-I isotherm with the micropore area and volume data of 158.3 m^2/g and 0.08 cm^3/g, respectively (Table S1 and Figure S2), comparable to those of AlPO-14,[30] while the Ar adsorption measurement gives a larger micropore area of 284.4 m^2/g and pore volume of 0.13 cm^3/g (Figure S3). The inconsistent results should be ascribed to the different dynamic diameters of N_2 (3.64 Å) and Ar (3.4 Å), and the small pore size of SAPO-14. Given that the dynamic diameters of most gas molecules are larger than 3.4 Å, it is supposed that some flat windows of SAPO-14 might be ineffective diffusion channels (e.g., the channel of 4.6 Å × 1.9 Å) for the methanol conversion reaction.

The SEM images of SAPO-14 are displayed in Figure 2A,B. The crystals have a flat morphology similar to that of AlPO-14.[30] The particle size is ca. 3 μm with a thickness of around 200 nm. TEM and selective area electron diffraction (Figure 2C,D) reveal that the slice can be indexed to the {001} crystal plane of the AFN structure, suggesting the short tunnel of SAPO-14 crystals along the *c*-axis.

Solid-state MAS NMR was used to investigate the status of the organic template and the framework-atom chemical environments of SAPO-14. The ^{13}C CP/MAS NMR spectrum gives two signals at 48.6 and 21.5 ppm attributed to the secondary and primary carbon atoms of the IPA template (Figure S4). This indicates that the IPA molecules remain intact in the product. The ^{27}Al and ^{31}P MAS NMR spectra of the as-synthesized and calcined SAPO-14 are complicated (Figure 3) but all of them resemble the reported MAS NMR spectra of AlPO-14, which have been well studied by various NMR technologies.[31,32] The ^{27}Al NMR signals of as-synthesized SAPO-14 appear at ca. 40, 15, and −9 ppm with

https://dx.doi.org/10.1021/acscatal.9b04703
ACS Catal. 2020, 10, 3741−3749

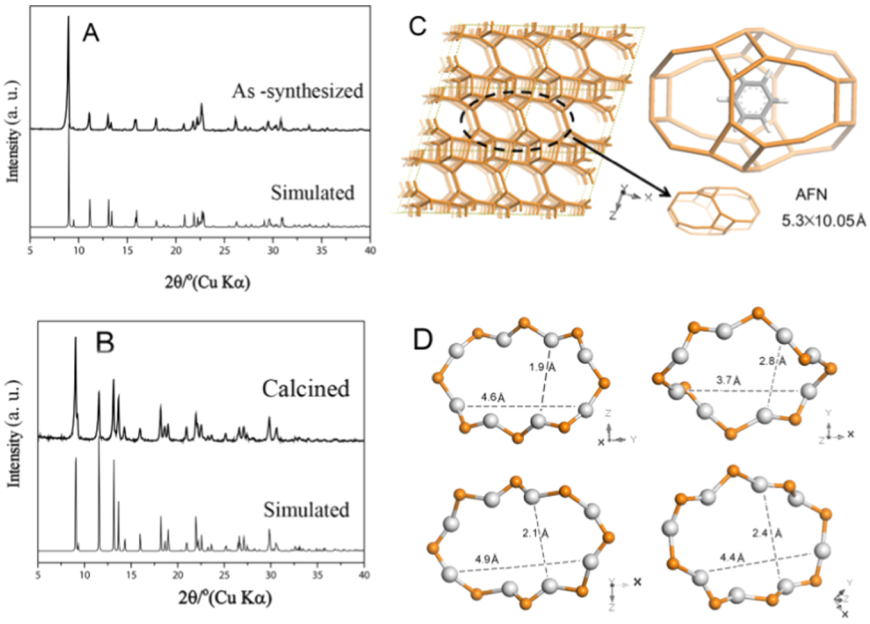

Figure 1. (A, B) Simulated and experimental XRD patterns of the as-synthesized and calcined SAPO-14. (C) AFN structure viewed along the [010] direction and $4^6 8^8$ AFN cage with a hexamethylbenzene located in (D) 8-MR pore openings of SAPO-14 in four directions.

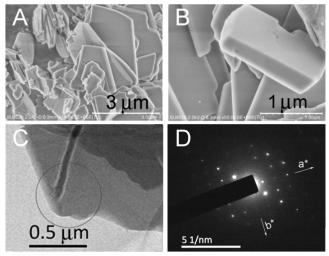

Figure 2. (A, B) SEM images of the calcined SAPO-14. (C, D) TEM image and selected area electron diffraction pattern of SAPO-14.

obviously second-order quadrupolar broadening. According to the literature, the three signals can be assigned to four-, five-, and six-coordinated Al species, respectively. After calcination, three ^{27}Al MAS NMR resonance peaks appear at about 40 ppm, indicating that all aluminum species are transformed to tetrahedral coordination. ^{31}P MAS NMR spectra of the as-synthesized SAPO-14 show four chemical shifts at −30, −25, −20, and −5 ppm attributed to four distinct P sites. After calcination, the environments of P atoms become similar, resulting in the overlapping of the signals from −20 to −40 ppm. An additional ^{31}P resonance at −18.5 ppm with very low intensity probably arises from an impurity also observed in the previous NMR investigation for AlPO-14.[32] The existence of the framework Si atom was verified by ^{29}Si MAS NMR (Figure 3). The ^{29}Si signals of as-synthesized SAPO-14, ranging from −85 to −120 ppm, are quite weak due to its low Si content (Figure S5). ^{29}Si CP MAS NMR was therefore measured, which gave four ^{29}Si chemical shifts at −80.8, −85.2, −89.2, and −92.1 ppm. The first three signals can be attributed to $Si(OAl)_2(OH)_2$, $Si(OAl)_3(OH)$, and $Si(OAl)_4$ species, respectively.[33] The last one may be due to $Si(OAl)_3(OSi)$ or $Si(OAl)_4$ at different T sites. After calcination, the ^{29}Si MAS NMR peak at around −92 ppm gets stronger. Two strong resonances at −92.5 and −95.3 ppm were assigned to Si(4Al) and Si(3Al) species, followed by weak peaks at ca. −100 and −109 ppm due to Si(*n*Al) (*n* = 2−0). The chemical shift at

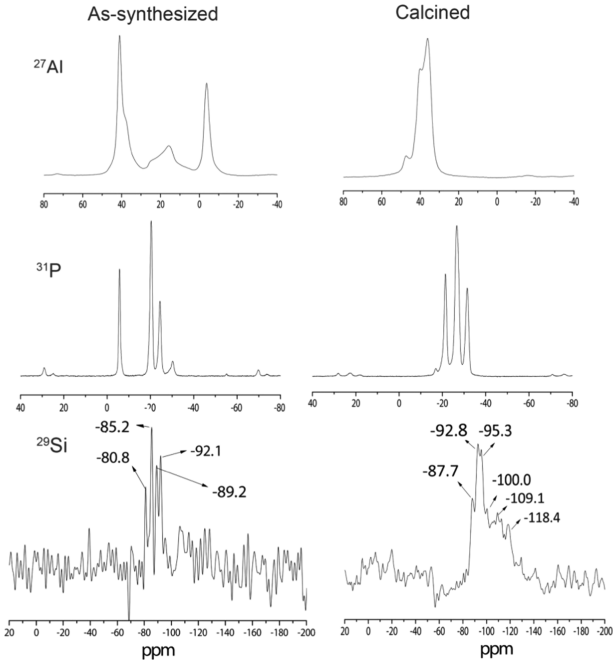

Figure 3. Solid-state ^{27}Al, ^{31}P, and ^{29}Si MAS NMR spectra of the as-synthesized (left) and calcined SAPO-14 (right). The ^{29}Si MAS NMR spectrum of the as-synthesized SAPO-14 is the ^{29}Si CP MAS NMR.

−118 ppm is ascribed to the existence of amorphous silica. The presence of surface silanol groups and amorphous silica in the ^{29}Si MAS NMR spectra suggests the difficulty in the substitution of the AlPO-14 framework atom by Si.

Acid sites were generated in SAPO-14 through Si incorporation, which was investigated by NH_3-TPD. The NH_3-TPD profiles present two NH_3 desorption peaks at ca. 160 and 360 °C, as seen in Figure 4. The former has quite a large peak area attributed to the desorption of physically absorbed NH_3 or NH_3 absorbed on the terminal hydroxyl groups with weak Brønsted acid sites. The latter is assigned to

https://dx.doi.org/10.1021/acscatal.9b04703
ACS Catal. 2020, 10, 3741−3749

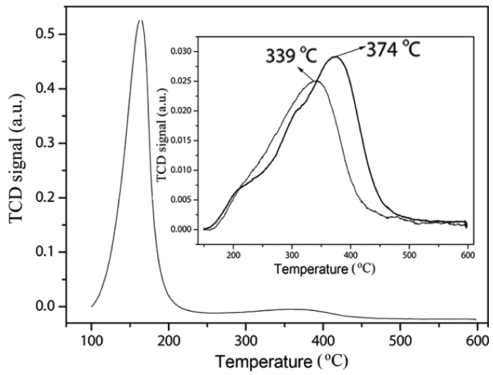

Figure 4. NH_3-TPD profiles of the SAPO-14. The inset is the NH_3-TPD profiles of SAPO-14 (dark line) and SAPO-18 (light line) adsorbing NH_3 at 150 °C.

the desorption of NH_3 from strong Brønsted acid sites. To better learn the acidity of SAPO-14, NH_3-TPD with NH_3 adsorption at a higher temperature (150 °C) was further performed to avoid the influence of the physically absorbed NH_3. For comparison, the NH_3-TPD of SAPO-18 with an approximate silica content (sample 6 in Table 1) was also investigated. The results are shown in the inset of Figure 4. The desorption temperature of SAPO-14 is higher than that of SAPO-18, possibly due to the narrower diffusion channels of the former. Their acid amounts are 0.25 and 0.20 mmol/g for SAPO-14 and SAPO-18, respectively, estimated based on the NH_3-desorption peak area.

3.2. Catalytic Performance of SAPO-14. The catalytic performance of SAPO-14 was evaluated by the methanol conversion (MTO) reaction, and the results of sample S2 are given in Figure 5. Under the reaction conditions of 450 °C and

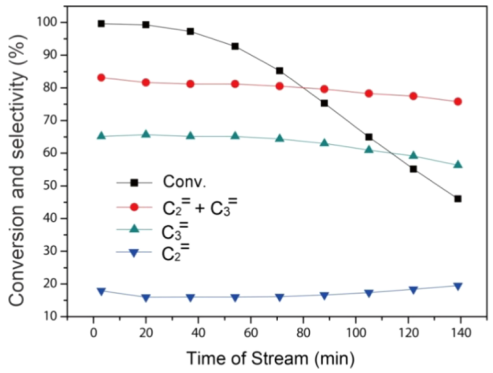

Figure 5. Methanol conversion and product selectivity as a function of time on stream over sample S2. The reaction conditions are 450 °C and WSHV = 0.5 h^{-1} with methanol partial pressures of 4.2 kPa.

methanol weight hour space velocity (WHSV) of 0.5 h^{-1}, the methanol conversion higher than 99% can be maintained for ca. 20 min, which drops to 85.3% at 71 min, and 55.1% at 122 min. The selectivity of ethylene plus propylene remains over 80% when the methanol conversion is higher than 85%. Notably, propylene selectivity is very high, with the largest value of 65.7% and a propylene/ethylene (P/E) ratio of 4.1 at TOS of 20 min. These data are much higher than those of SAPO-34 and SAPO-18 whose propylene selectivities are always less than 50% and the P/E ratio lower than 2.0.[22] More MTP zeolitic catalysts with a 10-ring or 12-ring channel system, including high-Si ZSM-5,[16] boron-containing CON,[18] and high-Si β,[19] were also compared with SAPO-14. Their structural features and optimal MTO catalytic results are summed up in Table 2. Comparatively, SAPO-14 has higher propylene, propylene plus ethylene, and lower C_{4+} selectivity than those of medium- and large-pore MTP catalysts. Moreover, the selectivity of methane on SAPO-14 is relatively high, which should be related to the rapid formation of coke species and deactivation. In view of the relatively short catalytic lifetime of SAPO-14, it is speculated that SAPO-14 might be a promising MTP catalyst for the fast fluidized-bed reactor, wherein highly initial olefin selectivity is critical and continuous regeneration of the deactivated catalyst can be realized.[1]

The influences of WHSV on the catalytic performance were investigated at 450 °C, and the results are shown in Figure S6. With the increase of WHSV, the catalytic lifetime displays a shortened trend, as expected, but the initial propylene selectivity (methanol conversion >90%) exhibits less variation together with the increased initial P/E ratio. The MTO reaction was thus further investigated at methanol WHSV of 2.0 h^{-1} but with different reaction temperatures. The reaction herein was carried out by intermittent feeding to obtain more reaction details (N_2 flow was purged during the interval of GC analysis). As seen in Figures 6A and S7, higher conversion can be achieved as the increased temperature. A short induction period appears at the reaction temperatures lower than 400 °C. It is noteworthy that the propylene selectivity is as high as 77.3% at TOS of 3 min, 400 °C (conversion: 89.2%, Figure 6B). In addition, there are 10.1% C_4 products followed by 8.0% ethylene and 2.2% methane. Among C_4 products, the butylene products occupy over 99.5%, including 61% *trans*-2-butene, 20% 1-butene, and 17.7% *cis*-2-butene, as illustrated in the inset of Figure 6B. Imposed by the severely steric constraints of SAPO-14, the intracrystalline diffusivity of iso-butylene should be significantly slower than that of linear butylenes, resulting in its negligible selectivity. Increasing or decreasing the reaction temperature leads to the descent of propylene selectivity and raised selectivity of methane, ethylene, and C_{4+} products. No matter how the conditions are changed, the P/E ratios remain high and the hydrogen transfer index (HTI) remains at a low level, as shown in Figure 6C. Taking into account methanol conversion, propylene selectivity, and P/E ratio altogether, the optimal reaction temperature for the SAPO-14 catalyzed MTP reaction should be 450 °C.

The regeneration ability of SAPO-14 is another important factor for its application. The deactivated catalyst was therefore calcined at 600 °C for 2 h (named R-SAPO-14) to retest its catalytic properties. The results are presented by hollow symbols in Figure 6. The catalytic performance of R-SAPO-14 changes little, confirming its good regeneration ability. In addition, the hydrothermal stability of SAPO-14 was evaluated. After steaming treatment at 750 °C for 10 h, the sample still maintains high crystallinity (Table S1), and its catalytic performance even shows a slight enhancement (Figure S8). These results confirm the potential application of the SAPO-14 catalyst for a fast fluidized-bed reactor, which requires excellent hydrothermal stability of the catalyst.

3.3. MTP Reaction Mechanism Investigation over SAPO-14. To understand the reason behind the high propylene selectivity of SAPO-14, nonacidic AlPO-14 and SAPO-18s with 0.6 and 2.0% Si contents were synthesized to investigate their MTO catalytic performances. The results are listed in Table 3 and Figure S9. The highest methanol

https://dx.doi.org/10.1021/acscatal.9b04703
ACS Catal. 2020, 10, 3741−3749

Table 2. Summary of MTP Catalyst Candidates and Their Representative Catalytic Results[a]

material	ZSM-5[16]	B-CON[18]	β[19]	SAPO-18[b]	SAPO-14[b]
topology	MFI	CON	BEA	AEI	AFN
channel structure	10-ring/3D	12-ring/3D	12-ring/3D	8-ring/3D	8-ring/3D
pore size (Å)	5.4 × 5.6	6.4 × 7.0	6.6 × 6.7	3.8 × 3.8	see Figure 1
compositions	Si/Al = 400	134	Si/Al = 277	$Al_{0.49}P_{0.49}Si_{0.02}$	$Al_{0.50}P_{0.48}Si_{0.02}$
conversion (%)	99.9	100	100	99.97	99.3
CH_4	1.0			0.4	5.6
C_2H_6	0.5			0.1	0.5
C_3H_8	0.8			0.4	0.8
$C_2^=$	4.2	4.5	5.9	30.4	15.9
$C_3^=$	51.0	60	58.3	45.3	65.7
$C_2^= + C_3^=$	55.2	64.5	64.2	75.7	81.6
C_{4+}	42.5	>30	>33.2	23.4	11.5
P/E ratio	12.1	>10	9.9	1.5	4.1

[a]The data of ZSM-5, B-CON, and β were collected from the literature. [b]The data are from our MTO catalytic results of sample S6 and sample S2 in Table 1. The points with the highest propylene selectivity were taken.

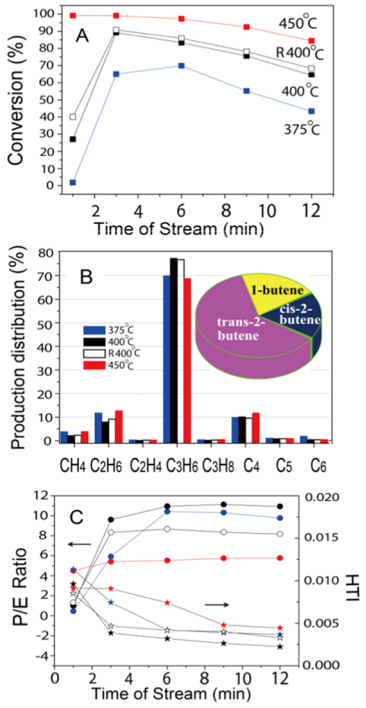

Figure 6. Methanol conversion as a function of time of stream (A), product distribution at TOS of 3 min (B), and P/E Ratio and HTI as a function of time of stream (C) over the SAPO-14 catalyst (sample S2) at various temperatures. The inset of (B) is the detail of C_4 product distribution at 400 °C, TOS = 3 min. Intermittent sampling was taken. Blue: 375 °C, black: 400 °C, red: 450 °C, R and hollow symbol refer to the regenerated sample. Methanol space velocity WHSV is 2.0 h^{-1} with methanol partial pressure of 16.8 kPa.

conversion for AlPO-14 is only 7.3%, with propylene selectivity of 47.2% and a P/E ratio of 3.1. The result suggests that the high propylene selectivity of SAPO-14 should be related to its enough acidity to catalyze the methanol conversion. When the acidity is too weak, the limited methanol conversion occurs both on the external surface and in the channels. Therefore, the high propylene selectivity achieved in the channel is offset by the external surface reaction resulting in moderate propylene selectivity. SAPO-18 with the 0.6% Si content (sample S5) gives comparable methanol conversion of 85.5% at 400 °C with that of SAPO-14 (sample S2). However, both propylene selectivity (47.4%) and the P/E ratio (1.9) are lower for SAPO-18, which continue to decrease when the Si content is further increased to 2% (sample S6). The results agree with the reports that SAPO-18 with lower acid density may promote the olefins cycle during the MTO reaction favoring the formation of more propylene.[22] Nevertheless, the propylene selectivity and P/E ratio on SAPO-18 are obviously inferior to those on SAPO-14. These results demonstrate that the high propylene selectivity of SAPO-14 strongly depends on its special AFN structure. Possibly, the larger AEI cage of SAPO-18 can easily accommodate the bulky aromatic intermediates, compared with the smaller AFN cage. The aromatic cycle thus occupies a higher proportion over SAPO-18 than on SAPO-14, leading to their difference in product selectivity.[11]

To confirm our conjecture, isotopic switch experiments were conducted to study the MTO reaction pathway over SAPO-14. ^{13}C-methanol was fed for 1 min after 2 min of ^{12}C-methanol reaction at 400 °C, WHSV of 2 h^{-1}. The TOS of 3 min was believed to be the point with the highest propylene selectivity and high methanol conversion based on the above results. The ^{13}C incorporation in the products, including both effluent and

Table 3. Catalytic Performance of AlPO-14 and SAPO-18 in the MTP Reaction[a]

samples	conv. (%)	$C_2^=$ (%)	$C_3^=$ (%)	$C_2^= + C_3^=$ (%)	C_4–C_6 (%)	P/E ratio	lifetime[b] (min)
S1-AlPO-14	7.3	15.2	47.2	62.4	32.1	3.1	
S5-SAPO-18-400 °C (0.6% Si)	85.5	25.1	47.4	72.5	26.7	1.9	
S6-SAPO-18-400 °C (2.0% Si)	100	30.4	45.3	75.7	23.4	1.5	310
S6-SAPO-18-450 °C (2.0% Si)	99.9	34.9	42.2	77.1	21.2	1.2	140

[a]Reaction conditions: temperature, 400 or 450°C, WHSV = 2 h^{-1} with methanol partial pressure of 16.8 kPa. The data are the points with the highest propylene selectivity. [b]Lifetime is defined as the period with methanol conversion larger than 99%. The highest methanol conversion on S5-400 °C is 88%.

https://dx.doi.org/10.1021/acscatal.9b04703
ACS Catal. 2020, 10, 3741−3749

hydrocarbons retained in SAPO-14 are analyzed by GC-MS, and the results are shown in Figure 7. In gas-phase products,

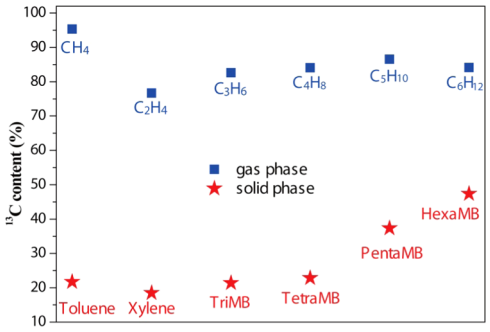

Figure 7. ^{13}C content in effluent and retained hydrocarbons in SAPO-14 at 400 °C after 2 min ^{12}C-methanol reaction, followed by 1 min ^{13}C-methanol reaction, WHSV = 2 h^{-1}.

methane and ethylene have 95 and 76.7% ^{13}C contents, respectively. C_3−C_6 alkenes have similar ^{13}C contents ranging from 82.6 to 86.6%. In contrast, the ^{13}C contents of the hydrocarbons confined in the catalyst, including toluene, xylene, tri-, tetra-, penta-, and hexa-MBs, are relatively low. The ^{13}C contents in toluene, xylene, tri-, and tetra-MB are comparable at around 20%, which increase to 37% for penta-MB and 47% for hexa-MB. The similar experimental results have also been observed on ZSM-22 zeolite.[13] More rapid incorporation of ^{13}C in alkene products than in the retained hydrocarbons suggests that the olefins-based route is dominant under the current reaction conditions. Since ethylene is the slowest one in getting methylated, the increase of the ^{13}C content will delay than other C_{3+} alkenes. Penta- and hexa-MB seem to be the most active aromatic species in the aromatics-based cycle, which benefits the generation of more propylene than ethylene.[21,22] However, this is hard to be well understood at the moment, given the small volume of the AFN cage.

Reaction-diffusion simulations on the MTP reaction over SAPO-14 and SAPO-18 catalysts were also conducted to further identify the reaction routes. The simulation is based on a reaction-diffusion simulation program developed by us recently.[34,35] The basic principle of this simulation is shown in Figure S10. The architecture−catalysis relationship is mainly reflected in the reaction kinetics and diffusion features. Maxwell−Stefan diffusion theory and ideal adsorbed solution theory are applied to a multi-component system. The effective diffusivities and Langmuir adsorption parameters in the Maxwell−Stefan diffusion theory[36] were measured by an intelligent gravimetric analyzer (IGA) technique. The reaction network was developed based on the dual-cycle mechanism and is shown in Table S2. Based on the results of the single zeolite crystal scale, the simulations of the fixed-bed reactor can be performed, which show good agreement with the experimental results of SAPO-14 and SAPO-18 (Figure S11). Analyzing the reaction kinetics reveals that the kinetic constants of the olefins-based cycle over SAPO-14 are obviously larger than those of the aromatics-based cycle (Table S2), indicating the dominant role of the olefins cycle in the SAPO-14-catalyzed reaction. Note that the kinetic constants of the aromatics-based cycle on SAPO-14 are also significantly lower than on SAPO-18. We deduce that the low reaction rate of the aromatics cycle on SAPO-14 should mainly result from the restriction of a low barrier "side-chain" route[37,38] by its small cage. Together with the low acidity of SAPO-14, the olefins-based cycle instead of the aromatics-based cycle is believed to be dominant in the MTO process. This result is consistent with the conclusion revealed by isotopic switch experiments.

The reaction-diffusion simulation was also expanded to investigate the effect of coke species on methanol diffusion, as shown in Table S3. It reveals that active hydrocarbons generated in SAPO-14, like monocyclic and bicyclic aromatics, would cause 40 times impact on the effective diffusion coefficients of methanol than SAPO-18, which explains well the short lifespan of the SAPO-14 catalyst. To better understand the deactivation process, various characterization techniques were conducted on the SAPO-14 catalyst exposed to methanol at 400 °C for 30 min (WHSV = 2 h^{-1}). N_2 adsorption measurement gives a micropore area of 14 m^2/g and a micropore volume of 0.007 cm^3/g (Table S1), suggesting a blockage of the catalyst channels. The organic compounds confined in the catalyst were analyzed by GC-MS, and the results were given in Figure S12. PolyMBs, including toluene, *m*-toluene, tri-MB, and tetra-BM, are the main compounds detected. The absence of penta-MB and hexa-MB might be attributed to their high activity regarding the highest ^{13}C content in penta-MB and hexa-MB among polyMBs retained in the catalyst (Figure 7). In addition, there is only a very small amount of naphthalene and tricyclic phenanthrene type compounds in the GC-MS chromatograms, showing that the formation of large aromatic compounds is seriously restricted by the small AFN cage. It is thus speculated that the obstacle of mass transfer in SAPO-14 is created following the formation and accumulation of hydrocarbons, which results in the fast catalyst deactivation.

Based on the above analysis, the catalytic performance of the SAPO-14 molecular sieve can be well understood, as illustrated in Figure 8. The ultra-small cage space, moderate acid strength,

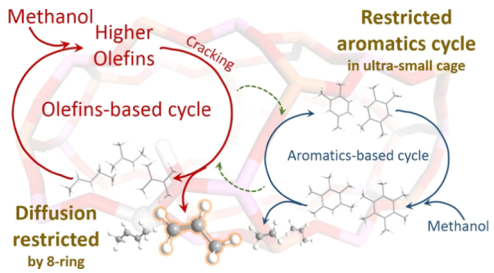

Figure 8. Supposed reaction mechanism of high propylene selectivity in methanol conversion over the SAPO-14 catalyst.

and low acid concentration of the SAPO-14 catalyst restrain the occurrence of the aromatics cycle and reduce the side reactions greatly, like cyclization and hydrogen transfer reactions, which encourage the olefins methylation/cracking pathway, resulting in significantly improved propylene selectivity. Moreover, the relatively narrow 8-ring pore openings limit the diffusion of C_{4+} products, which further contributes to the selective production of propylene.

4. CONCLUSIONS

In summary, a SAPO-14 molecular sieve with AFN topology has been hydrothermally synthesized for the first time, which exhibits extraordinary catalytic performance in methanol conversion to produce propylene. An unprecedentedly high

https://dx.doi.org/10.1021/acscatal.9b04703
ACS Catal. 2020, 10, 3741−3749

one-pass propylene selectivity and the propylene/ethylene ratio have been achieved. The SAPO-14 material exhibits excellent thermal and hydrothermal stability, which demonstrates it as a promising catalyst for the circulating fluidized-bed MTP reaction process. This work provides a protocol on propylene selectivity regulation for the MTO reaction, that is, by selecting the small-pore SAPO molecular sieve catalyst with an ultra-small cage, narrower 8-MR pore opening, and low acid concentration, an olefins-based route may dominate the methanol conversion process, which combines with the limited diffusion channel and thus maximizes the propylene selectivity. The current result opens up a new perspective on the design and synthesis of the zeolite catalyst. More work on catalyst optimization and in-depth understanding of the selectivity control principle of the zeolite-catalyzed methanol conversion process are still underway.

■ ASSOCIATED CONTENT

Supporting Information

The Supporting Information is available free of charge at https://pubs.acs.org/doi/10.1021/acscatal.9b04703.

Characterization and catalytic performances of SAPO molecular sieves, and the reaction-diffusion simulation results (PDF)

■ AUTHOR INFORMATION

Corresponding Authors

Peng Tian − *National Engineering Laboratory for Methanol to Olefins, Dalian National Laboratory for Clean Energy, Dalian Institute of Chemical Physics, Chinese Academy of Sciences, Dalian 116023, P. R. China*; Email: tianpeng@dicp.ac.cn

Zhongmin Liu − *National Engineering Laboratory for Methanol to Olefins, Dalian National Laboratory for Clean Energy, Dalian Institute of Chemical Physics, Chinese Academy of Sciences, Dalian 116023, P. R. China*; orcid.org/0000-0002-7999-2940; Email: liuzm@dicp.ac.cn

Authors

Miao Yang − *National Engineering Laboratory for Methanol to Olefins, Dalian National Laboratory for Clean Energy, Dalian Institute of Chemical Physics, Chinese Academy of Sciences, Dalian 116023, P. R. China*

Bing Li − *National Engineering Laboratory for Methanol to Olefins, Dalian National Laboratory for Clean Energy, Dalian Institute of Chemical Physics, Chinese Academy of Sciences, Dalian 116023, P. R. China*

Mingbin Gao − *National Engineering Laboratory for Methanol to Olefins, Dalian National Laboratory for Clean Energy, Dalian Institute of Chemical Physics, Chinese Academy of Sciences, Dalian 116023, P. R. China; University of Chinese Academy of Sciences, Beijing 100049, P. R. China*; orcid.org/0000-0002-7143-2658

Shanfan Lin − *National Engineering Laboratory for Methanol to Olefins, Dalian National Laboratory for Clean Energy, Dalian Institute of Chemical Physics, Chinese Academy of Sciences, Dalian 116023, P. R. China; University of Chinese Academy of Sciences, Beijing 100049, P. R. China*

Ye Wang − *National Engineering Laboratory for Methanol to Olefins, Dalian National Laboratory for Clean Energy, Dalian Institute of Chemical Physics, Chinese Academy of Sciences, Dalian 116023, P. R. China; College of Chemistry, Henan Institute of Advanced Technology, Zhengzhou University, Zhengzhou 450001, P. R. China*

Shutao Xu − *National Engineering Laboratory for Methanol to Olefins, Dalian National Laboratory for Clean Energy, Dalian Institute of Chemical Physics, Chinese Academy of Sciences, Dalian 116023, P. R. China*; orcid.org/0000-0003-4722-8371

Xuebin Zhao − *National Engineering Laboratory for Methanol to Olefins, Dalian National Laboratory for Clean Energy, Dalian Institute of Chemical Physics, Chinese Academy of Sciences, Dalian 116023, P. R. China; University of Chinese Academy of Sciences, Beijing 100049, P. R. China*

Peng Guo − *National Engineering Laboratory for Methanol to Olefins, Dalian National Laboratory for Clean Energy, Dalian Institute of Chemical Physics, Chinese Academy of Sciences, Dalian 116023, P. R. China*; orcid.org/0000-0001-5392-3915

Yingxu Wei − *National Engineering Laboratory for Methanol to Olefins, Dalian National Laboratory for Clean Energy, Dalian Institute of Chemical Physics, Chinese Academy of Sciences, Dalian 116023, P. R. China*

Mao Ye − *National Engineering Laboratory for Methanol to Olefins, Dalian National Laboratory for Clean Energy, Dalian Institute of Chemical Physics, Chinese Academy of Sciences, Dalian 116023, P. R. China*; orcid.org/0000-0002-7078-2402

Complete contact information is available at: https://pubs.acs.org/10.1021/acscatal.9b04703

Notes

The authors declare no competing financial interest.

■ ACKNOWLEDGMENTS

The authors thank the financial support from the National Natural Science Foundation of China (Nos. 21476228, 21676262 91745109, and 21991091) and the Key Research Program of Frontier Sciences, CAS (QYZDB-SSW-JSC040). The authors acknowledge the helpful discussion from Dr. Svetlana Mintova and Prof. Jihong Yu, and the collaboration in the framework of China-French joint laboratory "Zeolites".

■ REFERENCES

(1) Tian, P.; Wei, Y.; Ye, M.; Liu, Z. Methanol to Olefins (MTO): From Fundamentals to Commercialization. *ACS Catal.* **2015**, *5*, 1922−1938.

(2) Galadima, A.; Muraza, O. Recent Developments on Silicoaluminates and Silicoaluminophosphates in the Methanol-to-Propylene Reaction: A Mini Review. *Ind. Eng. Chem. Res.* **2015**, *54*, 4891−4905.

(3) Khanmohammadi, M.; Amani, S.; Garmarudi, A. B.; Niaei, A. Methanol-to-Propylene Process: Perspective of the Most Important Catalysts and Their Behavior. *Chin. J. Catal.* **2016**, *37*, 325−339.

(4) Koempel, H.; Liebner, W. Lurgi's Methanol to Propylene (MTP (R)) Report on a Successful Commercialisation. In *Studies in Surface Science and Catalysis*; Noronha, F. B.; Schmal, M.; SousaAguiar, E. F., Eds.; Natural Gas Conversion VIII, Proceedings of the 8th Natural Gas Conversion Symposium; Elsevier, 2007; Vol. *167*, pp 261−267.

(5) Zhu, J.; Cui, Y.; Chen, Y.; Zhou, H.; Wang, Y.; Wei, F. Recent Tesearches on Process from Methanol to Olefins. *J. Chem. Ind. Eng.* **2010**, *61*, 1674−1684.

(6) Olsbye, U.; Svelle, S.; Bjørgen, M.; Beato, P.; Janssens, T. V. W.; Joensen, F.; Bordiga, S.; Lillerud, K. P. Conversion of Methanol to Hydrocarbons: How Zeolite Cavity and Pore Size Controls Product Selectivity. *Angew. Chem., Int. Ed.* **2012**, *51*, 5810−5831.

(7) Xu, S.; Zhi, Y.; Han, J.; Zhang, W.; Wu, X.; Sun, T.; Wei, Y.; Liu, Z. Advances in Catalysis for Methanol-to-Olefins Conversion. In *Advances in Catalysis*; Song, C., Eds., 2017; Vol. *61*, pp 37−122.
(8) Li, J.; Wei, Y.; Chen, J.; Xu, S.; Tian, P.; Yang, X.; Li, B.; Wang, J.; Liu, Z. Cavity Controls the Selectivity: Insights of Confinement Effects on MTO Reaction. *ACS Catal.* **2015**, *5*, 661−665.
(9) Pinilla-Herrero, I.; Olsbye, U.; Marquez-Alvarez, C.; Sastre, E. Effect of Framework Topology of SAPO Catalysts on Selectivity and Deactivation Profile in the Methanol-to-Olefins Reaction. *J. Catal.* **2017**, *352*, 191−207.
(10) Yang, M.; Fan, D.; Wei, Y.; Tian, P.; Liu, Z. Recent Progress in Methanol-to-Olefins (MTO) Catalysts. *Adv. Mater.* **2019**, No. 1902181.
(11) Svelle, S.; Joensen, F.; Nerlov, J.; Olsbye, U.; Lillerud, K.-P.; Kolboe, S.; Bjørgen, M. Conversion of Methanol into Hydrocarbons over Zeolite H-ZSM-5: Ethene Formation is Mechanistically Separated From the Formation of Higher Alkenes. *J. Am. Chem. Soc.* **2006**, *128*, 14770−14771.
(12) Bjørgen, M.; Svelle, S.; Joensen, F.; Nerlov, J.; Kolboe, S.; Bonino, F.; Palumbo, L.; Bordiga, S.; Olsbye, U. Conversion of Methanol to Hydrocarbons over Zeolite H-ZSM-5: On the Origin of the Olefinic Species. *J. Catal.* **2007**, *249*, 195−207.
(13) Teketel, S.; Olsbye, U.; Lillerud, K.-P.; Beato, P.; Svelle, S. Selectivity Control Through Fundamental Mechanistic Insight in the Conversion of Methanol to Hydrocarbons over Zeolites. *Microporous Mesoporous Mater.* **2010**, *136*, 33−41.
(14) Sun, X.; Mueller, S.; Liu, Y.; Shi, H.; Haller, G. L.; Sanchez-Sanchez, M.; van Veen, A. C.; Lercher, J. A. On Reaction Pathways in the Conversion of Methanol to Hydrocarbons on HZSM-5. *J. Catal.* **2014**, *317*, 185−197.
(15) Erichsen, M. W.; Svelle, S.; Olsbye, U. H-SAPO-5 as Methanol-to-Olefins (MTO) Model Catalyst: Towards Elucidating the Effects of Acid Strength. *J. Catal.* **2013**, *298*, 94−101.
(16) Hu, S.; Shan, J.; Zhang, Q.; Wang, Y.; Liu, Y.; Gong, Y.; Wu, Z.; Dou, T. Selective Formation of Propylene From Methanol over High-Silica Nanosheets of MFI Zeolite. *Appl. Catal., A* **2012**, *445*−*446*, 215−220.
(17) Hu, S.; Gong, Y.; Xu, Q.; Liu, X.; Zhang, Q.; Zhang, L.; Dou, T. Highly Selective Formation of Propylene From Methanol over High-Silica EU-1 zeolite catalyst. *Catal. Commun.* **2012**, *28*, 95−99.
(18) Yoshioka, M.; Yokoi, T.; Tatsumi, T. Development of the CON-Type Aluminosilicate Zeolite and Its Catalytic Application for the MTO Reaction. *ACS Catal.* **2015**, *5*, 4268−4275.
(19) Zhao, X.; Wang, L.; Li, J.; Xu, S.; Zhang, W.; Wei, Y.; Guo, X.; Tian, P.; Liu, Z. Investigation of Methanol Conversion over High-Si Beta Zeolites and the Reaction Mechanism of Their High Propene Selectivity. *Catal. Sci. Technol.* **2017**, *7*, 5882−5892.
(20) Zhao, X.; Wang, L.; Guo, P.; Yan, N.; Sun, T.; Lin, S.; Guo, X.; Tian, P.; Liu, Z. Synthesis of High-Si Hierarchical Beta Zeolites Without Mesoporogen and Their Catalytic Application in the Methanol to Propene Reaction. *Catal. Sci. Technol.* **2018**, *8*, 2966−2974.
(21) Song, W.; Fu, H.; Haw, J. F. Supramolecular Origins of Product Selectivity for Methanol-to-Olefin Catalysis on HSAPO-34. *J. Am. Chem. Soc.* **2001**, *123*, 4749−4754.
(22) Chen, J.; Li, J.; Yuan, C.; Xu, S.; Wei, Y.; Wang, Q.; Zhou, Y.; Wang, J.; Zhang, M.; He, Y.; Xu, S.; Liu, Z. Elucidating the Olefin Formation Mechanism in the Methanol to Olefin Reaction over AlPO-18 and SAPO-18. *Catal. Sci. Technol.* **2014**, *4*, 3268−3277.
(23) Martínez-Franco, R.; Li, Z.; Martinez-Triguero, J.; Moliner, M.; Corma, A. Improving the Catalytic Performance of SAPO-18 for the Methanol-to-Olefins (MTO) Reaction by Controlling the Si Distribution and Crystal size. *Catal. Sci. Technol.* **2016**, *6*, 2796−2806.
(24) Padin, J.; Rege, S. U.; Yang, R. T.; Cheng, L. S. Molecular Sieve Sorbents for Kinetic Separation of Propane/Propylene. *Chem. Eng. Sci.* **2000**, *55*, 4525−4535.
(25) Girnuse, I.; Löffler, E.; Louse, U.; Neissendorfer, F. Small Pore AlPO/SAPO Structures Formed in Dependence on the Silicon Content of the Synthesis Gel. *Collect. Czech. Chem. Commun.* **1992**, *57*, 946−958.
(26) Chen, J.; Thomas, J. M.; Wright, P. A.; Townsend, R. P. Silicoaluminophosphate Number-18 (SAPO-18)-A New Microporous Solid Acid Catalytst. *Catal. Lett.* **1994**, *28*, 241−248.
(27) Fan, D.; Tian, P.; Xu, S.; Xia, Q.; Su, X.; Zhang, L.; Zhang, Y.; He, Y.; Liu, Z. A Novel Solvothermal Approach to Synthesize SAPO Molecular Sieves Using Organic Amines as the Solvent and Template. *J. Mater. Chem.* **2012**, *22*, 6568.
(28) Wang, D.; Xu, S.; Yang, M.; Chu, Y.; Tian, P.; Liu, Z. Microporous Aluminophosphate ULM-6: Synthesis, NMR Assignment, and Its Transformation to $AlPO_4$-14 Molecular Sieve. *J. Phys. Chem. C* **2016**, *120*, 11854−11863.
(29) http://www.iza-structure.org/databases/.
(30) Zhao, X.; Xu, X.; Sun, L.; Zhang, L.; Liu, X. Adsorption Behavior of Carbon Dioxide and Methane on $AlPO_4$-14: A Neutral Molecular Sieve. *Energ Fuel* **2009**, *23*, 1534−1538.
(31) Ashbrook, S. E.; Cutajar, M.; Pickard, C. J.; Walton, R. I.; Wimperis, S. Structure and NMR Assignment in Calcined and As-Synthesized Forms of AlPO-14: A Combined Study by First-Principles Calculations and High-Resolution ^{27}Al -^{31}P MAS NMR correlation. *Phys. Chem. Chem. Phys.* **2008**, *10*, 5754−5764.
(32) Antonijevic, S.; Ashbrook, S. E.; Biedasek, S.; Walton, R. I.; Wimperis, S.; Yang, H. X. Dynamics on the Microsecond Timescale in Microporous Aluminophosphate AlPO-14 as Evidenced by ^{27}Al MQ MAS and STMAS NMR Spectroscopy. *J. Am. Chem. Soc.* **2006**, *128*, 8054−8062.
(33) Wang, C.; Yang, M.; Tian, P.; Xu, S.; Yang, Y.; Wang, D.; Yuan, Y.; Liu, Z. Dual Template-Directed Synthesis of SAPO-34 Nanosheet Assemblies with Improved Stability in the Methanol to Olefins Reaction. *J. Mater. Chem. A* **2015**, *3*, 5608−5616.
(34) Gao, M.; Li, H.; Yang, M.; Zhou, J.; Yuan, X.; Tian, P.; Ye, M.; Liu, Z. A Modeling Study on Reaction and Diffusion in MTO Process over SAPO-34 Zeolites. *Chem. Eng. J.* **2019**, *377*, No. 119668.
(35) Li, H.; Ye, M.; Liu, Z. A Multi-Region Model for Reaction-Diffusion Process within a Porous Catalyst Pellet. *Chem. Eng. Sci.* **2016**, *147*, 1−12.
(36) Krishna, R. Diffusion in Porous Crystalline Materials. *Chem. Soc. Rev.* **2012**, *41*, 3099−3118.
(37) Wang, S.; Chen, Y.; Wei, Z.; Qin, Z.; Ma, H.; Dong, M.; Li, J.; Fan, W.; Wang, J. Polymethylbenzene or Alkene Cycle? Theoretical Study on Their Contribution to the Process of Methanol to Olefins over H-ZSM-5 Zeolite. *J. Phys. Chem. C* **2015**, *119*, 28482−28498.
(38) De Wispelaere, K.; Hemelsoet, K.; Waroquier, M.; Van Speybroeck, V. Complete Low-Barrier Side-Chain Route for Olefin Formation During Methanol Conversion in H-SAPO-34. *J. Catal.* **2013**, *305*, 76−80.

https://dx.doi.org/10.1021/acscatal.9b04703
ACS Catal. 2020, 10, 3741−3749